# TITLE: Near-IR Sintering of Conductive Silver

# Nanoparticle Ink with In Situ Resistance Measurement

## AUTHOR NAMES

David Keller, Krystopher S. Jochem, Wieslaw J. Suszynski, Lorraine F. Francis\*

### **AUTHOR ADDRESS**

Department of Chemical Engineering and Materials Science, University of Minnesota, 421 Washington Avenue S.E., Minneapolis, Minnesota 55455, United States

## **KEYWORDS**

Infrared Sintering, Silver Nanoparticle Ink, In Situ Resistance Measurements, Aerosol Jet Printing

# ABSTRACT

Metal nanoparticle inks are excellent options for printing low-resistance metal conductors and electrical interconnects. However, after deposition, these inks require high-temperature annealing to sinter and increase conductivity. Infrared (IR) heaters are an efficient, roll-to-roll compatible method to apply thermal energy. Here, we characterize a near-infrared (N-IR) heater's effects on the structure and properties of printed silver nanoparticle ink (UTD Ag40x, UT Dots Inc.). A method was developed to measure the resistance and temperature of printed conductive inks as a function of exposure to the IR heater. The N-IR heater was found to sinter the Ag40x silver samples (lower the resistance of 7 mm printed lines to  $1000 \Omega$ ) in  $11.6 \pm 1.5$  min at maximum

intensity with a large drop from the highest measured resistance (60 M $\Omega$ ) to 1000  $\Omega$  in 1.2 ± 0.2 min. Decreasing the heater power increased the time to reach 1000  $\Omega$  (to 28.3 ± 2.0 min at 80%), but reducing from 60 M $\Omega$  to 1000  $\Omega$  still only takes 1.9 ± 0.3 min. This suggests sintering progresses rapidly once initiated. SEM images of the ink before and after IR heating show microstructural changes associated with sintering and indicate the role of agglomerates and organic binders in impeding sintering.

### TEXT

## **Introduction:**

Metal conductors act as interconnects between components and transmit power throughout electronic circuits. For flexible electronics, conductor fabrication by printing processes is an efficient alternative to traditional, subtractive fabrication techniques, which generate a significant amount of waste.<sup>1,2</sup> Printing has been demonstrated for the fabrication of a wide variety of electrical components, including sensors, RFID antennas, and solar cells.<sup>3–6</sup> All of these applications require printed electrical conductors. Silver nanoparticle inks are widely used as a starting material for fabricating these metal conductors. However, after deposition, nanoparticle inks require thermal processing to remove solvents and organic binders, and coalesce the silver nanoparticles into a cohesive, conductive film.<sup>7</sup> Melting of the silver nanoparticles requires a temperature too high for most plastic, flexible substrates so sintering is used as a lower temperature procedure to lower the resistance.<sup>8</sup>

Sintering is a thermally activated process that densifies a packed assembly of small particles into a polycrystalline solid.<sup>9</sup> During heating, the nanoparticles lower their free energy by diffusion processes that form contacts or necks between particles.<sup>10</sup> The particle assembly

densifies and individual particles become grains separated by grain boundaries.<sup>9</sup> For silver nanoparticle inks, heating also removes organic binders that coat the surface of the particles.<sup>2</sup> These processing steps require the application of thermal energy. There are several methods for heating, including ovens, infrared (IR) heaters, and photonic sintering systems.

An IR heater emits electromagnetic waves in the range of  $0.7~\mu m$ - $400~\mu m$ . <sup>11</sup> The radiation is emitted from the source and hits the sample without significantly heating the surrounding air, unlike a conventional heater. Incident IR excites the molecules in the target substance, causing vibrations and an increase in temperature. <sup>11</sup>

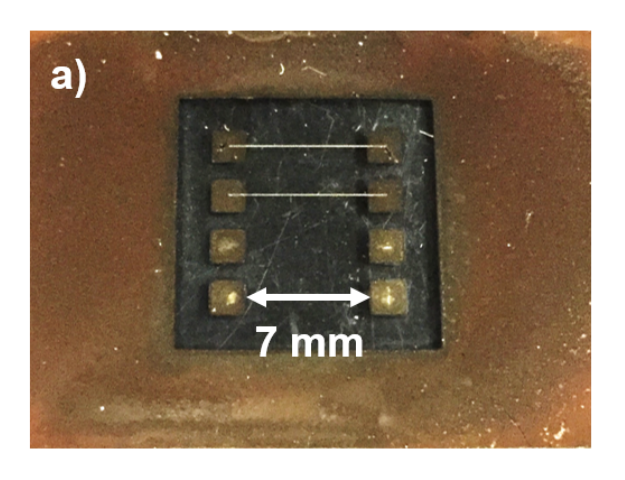
IR heaters are of interest for sintering of nanoparticle inks for several reasons. These heaters are compatible with roll-to-roll processing, capable of achieving high power densities, and relatively low in cost compared to other heating systems. 10,11 Compatibility with roll-to-roll processing allows for large-scale, economical manufacturing of devices. Also, polymer substrates commonly used in roll-to-roll processing do not have a strong absorbance in the IR and near infrared (N-IR) range of the electromagnetic spectrum. This suggests that inks can be sintered without degrading the plastic webs. 12

Past work on IR sintering of metal nanoparticle inks shows promising results with some reports documenting sintering in seconds to minutes.<sup>10,12</sup> The structural property changes and the development of electrical properties are of interest for better understanding the sintering process. Additionally, *in situ* electrical measurements during sintering have been shown to provide a unique understanding of how the sintering process progresses by analyzing the electrical resistance of the sample.<sup>13</sup> In this work, we have analyzed the sintering of a silver nanoparticle ink by a N-IR heater by *in situ* electrical resistance measurements during heating to better understand sintering performance.

# **Experimental Methods and Materials:**

Aerosol Jet Printing of Silver Ink

Aerosol jet printing was used to deposit silver nanoparticle lines onto glass slides. To facilitate electrical characterization, gold contact pads were first prepared on the glass slides by gold sputter deposition (Fullam EMS-76) through a shadow mask. See Figure 1a. The contact pads were 2 mm x 2 mm squares separated by 7 mm. Silver nanoparticle ink (UTD Ag40X, UT Dots Inc.) was used to print conductors between the centers of the contact pads for sintering studies. This ink contains ~ 40 wt% silver nanoparticles (~10 nm in diameter) with organic stabilizers dispersed in xylenes.<sup>7,14</sup> The ink was prepared for printing by adding 15% by volume terpineol. Terpineol acts as a cosolvent and lowers the surface tension of the silver ink, which assists with the formation of small aerosol particles.<sup>7,15,16</sup> The ink was then printed with an aerosol jet printer (AJ 100, Optomec) using a 150 µm nozzle, a carrier gas flow of 10 standard cubic centimeters per minute, sccm (10 sccm corresponds to 0.17 cm<sup>3</sup>/s at standard temperature and pressure) and a sheath gas flow of 60 sccm (1 cm<sup>3</sup>/s at standard temperature and pressure). The printing speed was 1 mm/s and the stage was heated to 50 °C to promote solidification of the ink when it contacts the substrate. Figure 1b shows an example height profile of a printed line characterized by a KLA-Tencore P-16 stylus profilometer.



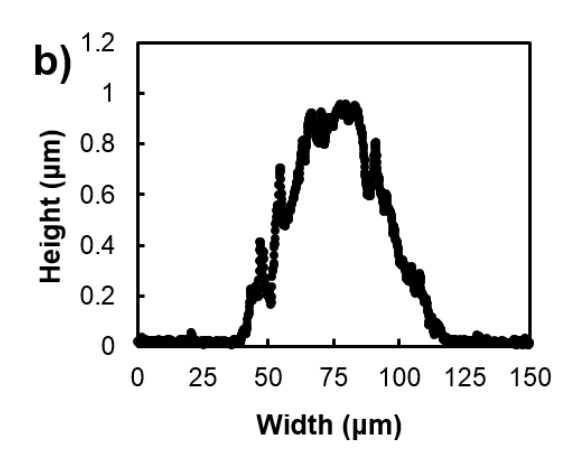


**Figure 1:** (a) Aerosol Jet Printed silver lines and gold contact pads, and (b) height profile of a printed conductor used to test the IR sintering systems.

# IR Sintering of Silver Ink

The IR heater assembly with features annotated is shown in Figure 2a. The sample was placed 12.9 cm below the face of the heater on a gold reflector. The reflector ensures that IR waves transmitted through the substrate are reflected back onto the sample. A custom probe system was used to contact the gold contact pads during heating so that real-time resistance could be recorded (Figure 2b). Springs in the probes kept the tips in contact with the sample. Resistance was measured with a digital multimeter (BK Precision, Model 393), which was connected to a computer and accessed with BK Precision Test Bench software. Resistance was measured from the time that the heater was turned on, through the sintering process, and after the heater was turned off.

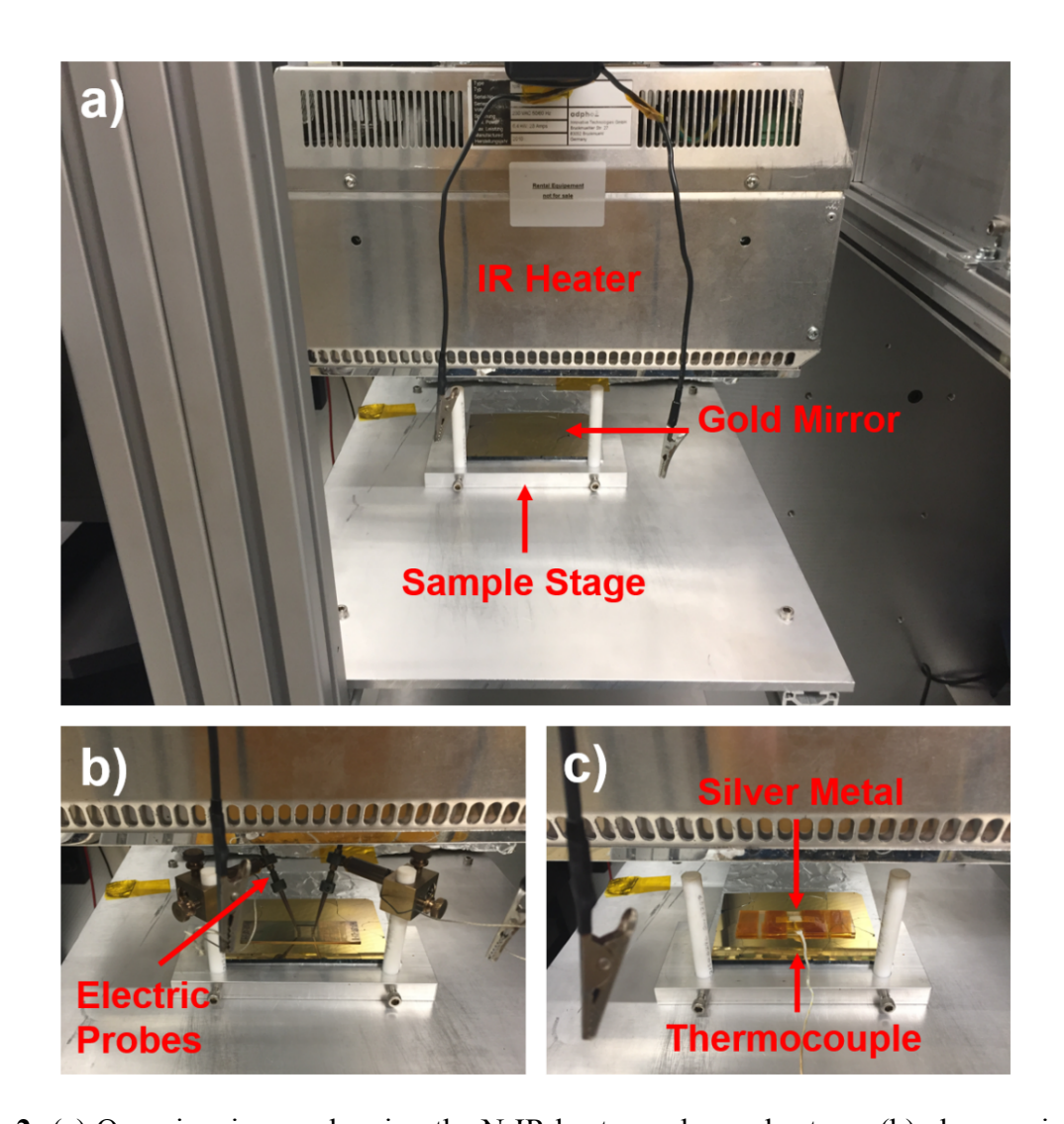


**Figure 2:** (a) Overview image showing the N-IR heater and sample stage, (b) close up image of the probe system used to measure electrical resistance during sintering, and (c) close up image of the assembly used to measure sample temperature during IR sintering.

An Adphos N-IR heater (model NIR120 M3, Innovative Technologies GmbH) was used in these studies. The heater emits at near infrared wavelengths, which are on the shorter side of the infrared spectrum with a peak wavelength of  $0.8 \mu m$ .<sup>17</sup> The Adphos heater has an effective heating area of 124 mm x 337 mm (measured at the base of the built-in reflector) and a power consumption of 5.1 kW at 100% power as measured by an Amprobe AMP-320 clamp meter. The heater has adjustable power output from 1 to 100%. At 100% power, the N-IR heater has a power

output as calculated from the input electrical power and the opening on the heater of 122 kW/m<sup>2</sup>. The efficiency of the heater is unknown, so all power levels reported in this paper are based on the electrical input power of the heater.

# *Temperature Monitoring*

To estimate the sample temperature during the sintering process, a piece of silver with dimensions of 5 mm x 25 mm and 1 mm thick with a thermocouple attached to the back side was placed at the same distance from the N-IR heater as the printed samples. The top surface of the silver sample was aerosol jet printed with the same silver ink used for the conductors to provide IR absorption similar to the printed silver lines. For support, the silver piece was attached to a glass slide with Kapton tape, as shown in Figure 2c. The assembly was placed on the gold reflector during the test to further simulate the sintering conditions for the silver conductors. Thermocouple temperature data were recorded by a BK Precision Model 393 multimeter with a type K thermocouple.

# Scanning Electron Microscopy of Silver Ink

Scanning Electron Microscope (SEM) imaging was used to characterize the physical changes in the silver nanoparticle lines after IR heating. SEM images were obtained using a Hitachi S4700 field emission SEM.

## **Results and Discussion**

### Resistance Measurements

Figure 3 shows results from *in situ* resistance measurements performed during N-IR heating at 100 % power. In all cases, the heater was turned on at time 0. Initially, the resistance of all lines was greater than the 60 M $\Omega$  resistance measurement limit of the equipment. After turning on the heater, it takes some time before the resistance drops below this limit. This delay

is possibly due to the burnout of the organic binder in addition to sintering. The displayed data begins when the resistance of the samples drops below  $60~\mathrm{M}\Omega$ . The onset of measurable resistance in the UTD Ag40x ink occurred at  $\sim 10.3 \pm 1.6~\mathrm{min}$  with the heater at 100 % and a sample to heater distance of 12.9 cm. Although these overall heating times for sintering are significantly longer that those reported for some other custom ink formulations  $^{12}$ , the time is actually faster than those reported for conventional oven sintering techniques using the same aerosol jet printed silver nanoink used in our studies.  $^{7,18-20}$  Moreover, the set-up required for this study has a larger distance between the IR source and the sample than is typical, which may also lead to the longer times. Interestingly, once the resistance becomes measurable ( $60~\mathrm{M}~\Omega$ ), it drops rapidly to a value of less than  $100~\Omega$ . This result suggests that at some stage, the sintering process becomes rapid and conductivity develops rapidly. It is important to note that the internal resistance of the measurement system is only on the order of  $3~\Omega$ , so it does not significantly affect the measured resistance values. Fluctuations in the resistance value of the sintered conductors were observed after the resistance leveled off. This is possibly due to the presence of a cooling fan in the heater.

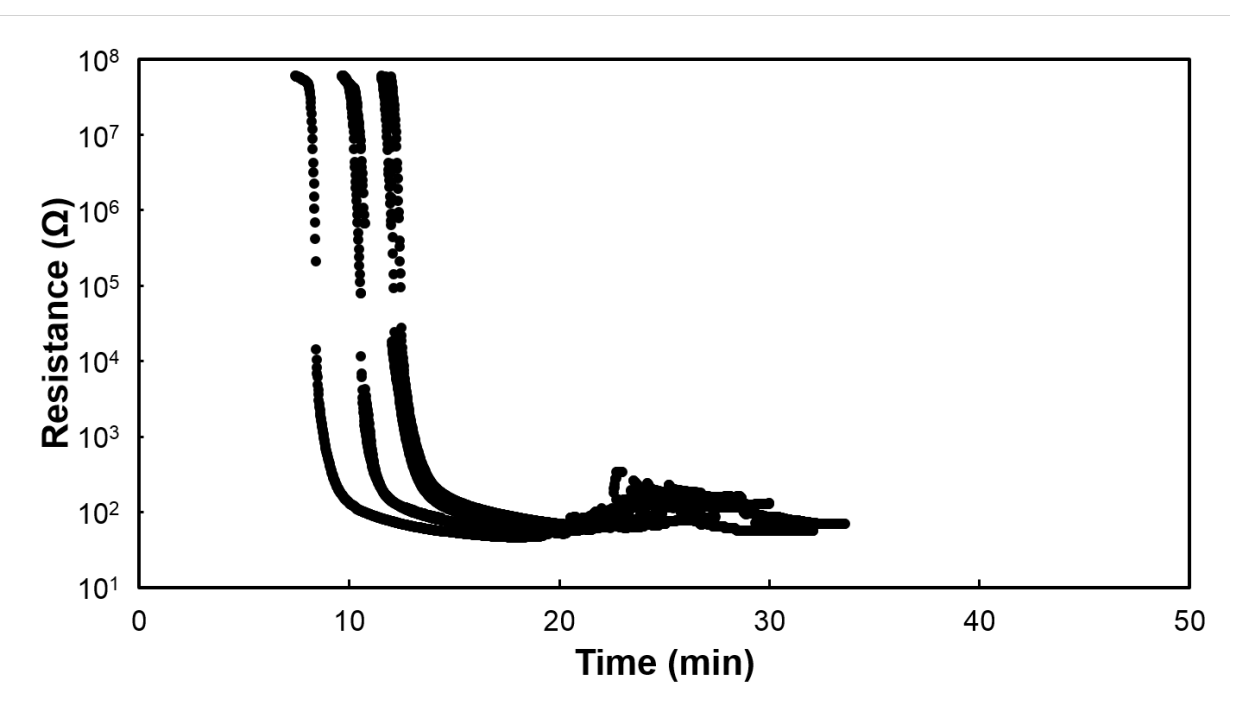


**Figure 3:** *In situ* resistance measurements of lines printed with UTD Ag40x silver ink for six experiments with the N-IR heater at 100% power and a sample to heater distance of 12.9 cm.

The bulk property of resistivity can be used to compare the properties of the sintered metals without any effects from the geometry of the printed features. Resistivity,  $\rho$ , is defined as:

$$\rho = \frac{R*A_c}{L} \tag{1}$$

where R is the measured resistance,  $A_c$  is the cross-sectional area of the line, and L is the length of the line. The cross-sectional area was estimated from profilometry scan data. During sintering, the resistivity of the wire decreases. With the N-IR heater at 100 % power, a minimum  $\rho$  of 18.0  $\pm$  1.8  $\mu\Omega$ •cm was achieved for the lines printed from UTD Ag40x silver ink. The sintered silver resistivity value is higher than that of bulk silver (1.51  $\mu\Omega$ •cm) and higher than the reported resistivity of other sintered silver nanoparticle inks, suggesting that complete binder burnout may not have occurred or the porosity of the sintered silver is significant.<sup>7,10</sup> This hypothesis is further supported by the SEM characterization discussed later in this paper.

Since the power output level of the N-IR heater can be varied, tests were carried out to analyze its sintering performance at different power levels. The sintering performance was observed to depend strongly on the power level of the heater. The times required to reduce the resistance of the printed silver conductors to  $1000~\Omega$  for each of the power levels are shown in Table 1. As the power level of the heater decreased, the time at which the silver ink samples became conductive increased dramatically. When the power level of the N-IR heater was reduced from 80% to 70%, the length of time required for the samples to sinter more than doubled, and the sintering performance became much less consistent as observed in the large increase in the standard deviation. The results suggest that a power level of  $\sim$ 80% is the minimum reliable power for sintering the aerosol jet printed silver conductors with the configuration of our system.

Table 1 also reports the time required for the printed samples under the N-IR heater to reduce from  $60 \text{ M}\Omega$  (the maximum resistance our system can measure) to  $1000 \Omega$ . Interestingly, these times are a small fraction of the total sintering time and only increase slightly as power level is decreased to 80%. This result further suggests that once sintering begins, it progresses rapidly. The time required at 70% power to reduce the resistance from  $60 \text{ M}\Omega$  to  $1000 \Omega$  is significantly longer, which further indicates that 80% power is the minimum reliable power for sintering the UTD Ag40x silver ink in our system.

**Table 1:** Sintering performance of lines printed with UTD Ag40x silver ink with the N-IR heater at different power levels and a sample to heater spacing of 12.9 cm.

Power	Time to reach 1000 $\Omega$ (min)*	Time from 60 M $\Omega$ to 1000 $\Omega$ (min)*
100%	11.6 ± 1.5	$1.2 \pm 0.2$
90%	$18.6 \pm 2.0$	$1.4 \pm 0.7$
80%	$28.3 \pm 2.0$	$1.9 \pm 0.3$
70%	$65.1 \pm 20.0$	$8.8 \pm 4.3$

<sup>\*</sup>Results based on 5 or 6 samples with errors of one standard deviation

# Temperature Changes During Sintering

To better understand the relationship between the heater power and sintering performance, a series of temperature monitoring experiments were performed with the N-IR heater at varied power settings. These experiments were carried out on aerosol jet printed patch on a bulk silver substrate to ensure thermal contact with the thermal couple. Therefore, the temperatures measured are approximations of the specimens printed on glass. As shown in Figure 4a, the temperature measured at the substrate for all power settings increases rapidly during the first two minutes or so of N-IR heating, then more slowly before eventually plateauing. The final temperature increases approximately linearly with the power setting as shown in Figure 4b. Despite this linear trend, the required sintering time was not found to linearly depend on power setting (Table 1). This result is consistent with the thermally activated nature of both the decomposition of organic binder and sintering. Also, the relatively rapid increase in sample temperature at each power level confirms that the long delay before measurable resistance is observed in the printed conductors is not due to time required for the sample to heat up.

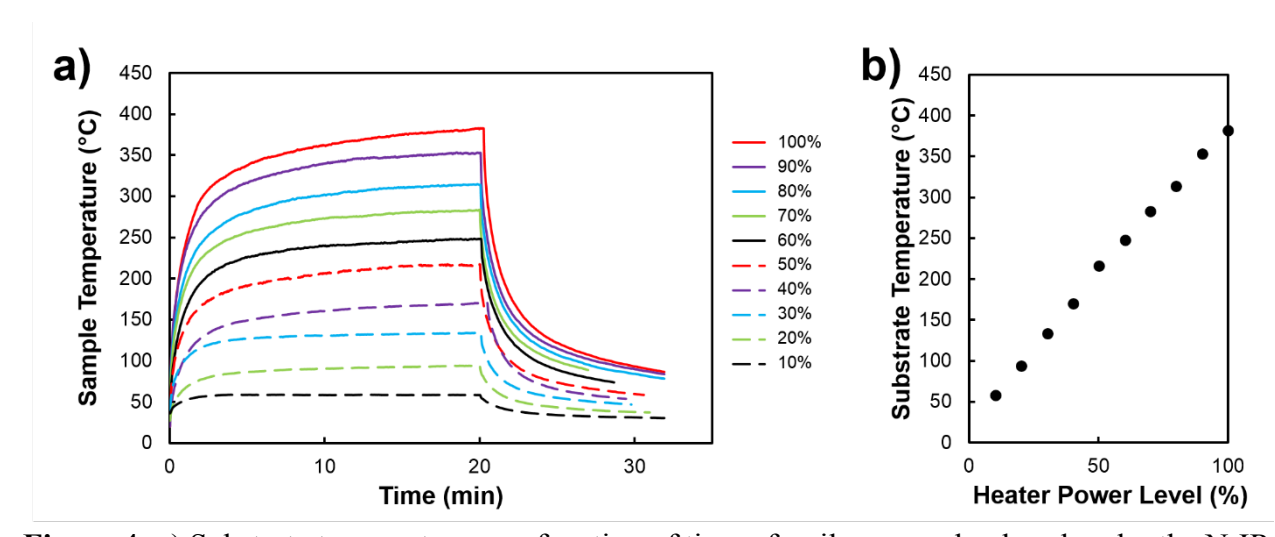


**Figure 4:** a) Substrate temperature as a function of time of a silver sample placed under the N-IR heater at the specified power levels with a substrate to heater spacing of 12.9 cm. The heater was turned off after 20 minutes. b) Substrate temperature after 20 minutes of heating as a function of heater power level.

### SEM Characterization

SEM images taken before and after sintering of the UTD Ag40x silver ink are shown in Figure 5. Significant physical changes are observed in the inks after sintering. The before sintering aerosol jet printed samples (Fig. 5 c and d) show ~500 nm particles, which are likely solidified clusters of the 10 nm nanoparticles. SEM images of drop-cast and un-sintered samples of the silver UTD Ag40x ink are also shown in Figure 5 (a and b). These drop-cast samples do not show the same formation of ~500 nm clusters, which strongly suggests the aerosol jet printing process is the source of these features. Williams, et al.<sup>21</sup> also noticed similar clusters in aerosol jet printed copper zinc tin sulfide nanoparticle inks and based on a study of deposition parameters, attributed the clusters to drying of mist droplets during transport. The added terpineol does not appear to have any effect on the cluster formation as drop-cast specimens prepared with or without terpineol were nearly identical and did not contain clusters. The clusters of the silver nanoparticles also appear to be surrounded by organic binders (Fig. 5d). On heating, these structures persist (eg. Fig. 5 e and f), but the spaces between them decrease, presumably as the organics depart. Additionally, individual nanoparticles become apparent in the microstructures of samples created using heating conditions that led to significant resistance drops (e.g., Figures 5 g-j), indicating that organic binder is pyrolyzed. Overall, densification is incomplete based on the void spaces observed between the silver grains after sintering. This result is consistent with the electrical measurements demonstrating higher than bulk resistivity and relatively long IR sintering times compared to studies with other nanoparticle inks.

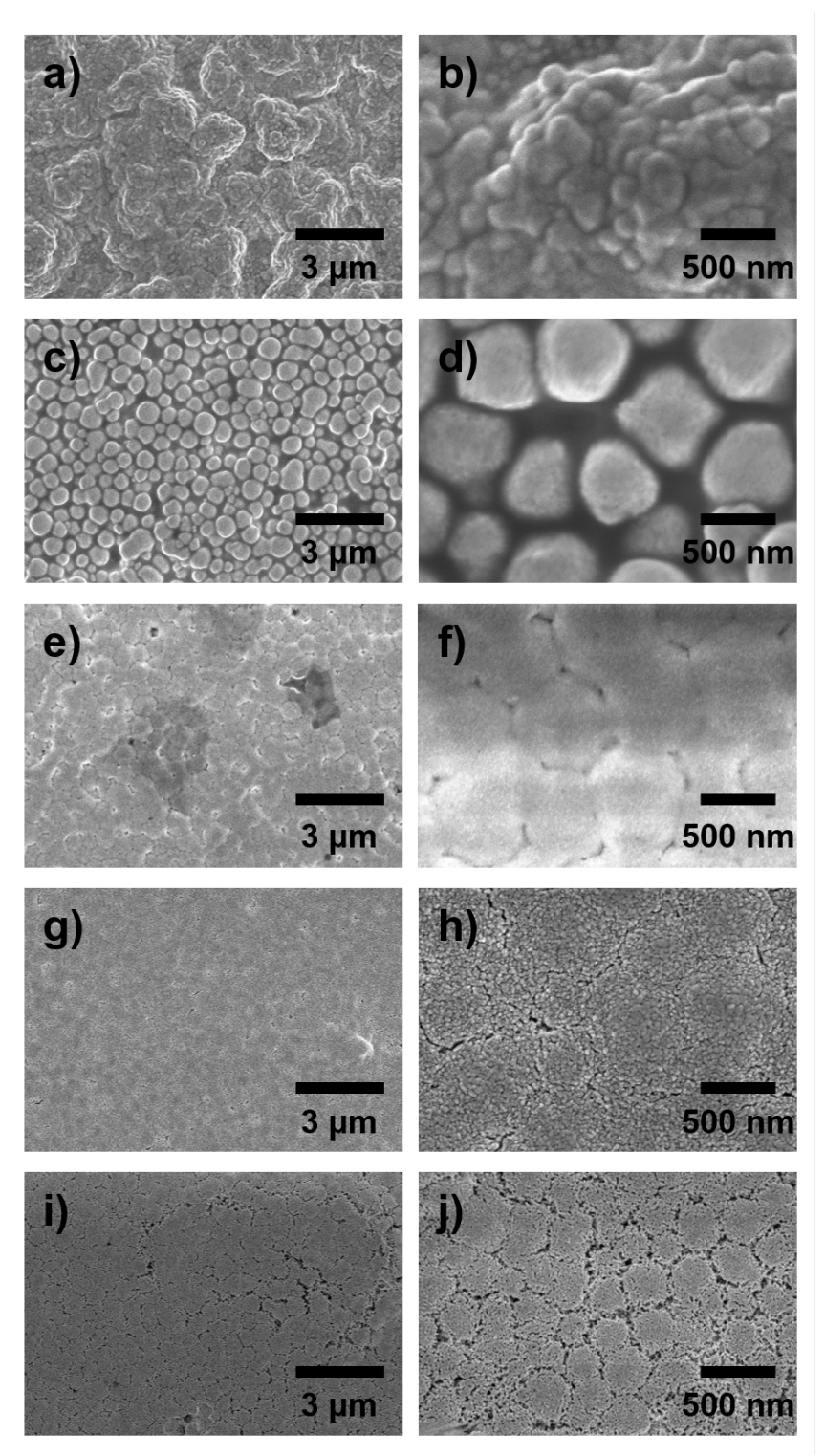


**Figure 5:** Pre and Post sintering SEM images of printed UTD Ag40x silver ink samples after various sintering conditions: (a) and (b) drop-cast and imaged before sintering, (c) and (d) aerosol jet printed and imaged before sintering, (e) and (f) aerosol jet printed and imaged after 20 minutes sintering with N-IR at 60%, (g) and (h) aerosol jet printed and imaged after 20 minutes sintering with N-IR at 80%, (i) and (j) aerosol jet printed and imaged after 20 minutes sintering with N-IR at 100%.

## **Conclusions**

The IR sintering of UTD Ag40x silver nanoparticle ink was studied with a unique system to measure the resistance of printed metal lines during the sintering process. This setup allowed measurement of changes in the electrical properties of the printed material during the sintering process. The *in situ* data showed that there is an initial delay in the appearance of conductivity, then a rapid increase in conductivity, and finally a plateau where further significant changes in conductivity are not observed. Increasing the power level of the N-IR heater system leads to a linear increase in the temperature achieved during heating, which is observed to lead to a faster sintering. Although a linear trend in sample temperature was observed with increasing the heater power, this did not correspond to a linear decrease in the required time to sinter silver ink samples, and ~80% power was required for achieving high conductivity silver lines. Microstructural studies showed that removal of organic binders and agglomerated nanoparticle structures in the printed material impede sintering. The techniques discussed here to sinter and characterize the progress of N-IR sintering can be applied to a wide variety of electrically conductive inks. Overall, IR heating successfully sinters conductive silver inks and the in situ measurement technique demonstrated here provides an efficient strategy for understanding the connections between processing conditions and property development.

## Acknowledgements

This work was initially supported by the Multi-University Research Initiative (MURI) program sponsored by the Office of Naval Research (MURI Award No. N00014-11-1-0690) and then by the National Science Foundation (NSF Award No. CMMI-1634263). K. S. J. gratefully acknowledges support from the NSF Graduate Research Fellowship Program under Grant No. (00039202). The authors thank F. Zare Bidoky for significant help with aerosol jet printing. The

authors thank Adphos North America for providing the Adphos IR heater used in these studies. Parts of this work were carried out in the Characterization Facility, University of Minnesota, which receives partial support from NSF through the MRSEC program. Portions of this work were conducted in the Minnesota Nano Center, which is supported by the National Science Foundation through the National Nano Coordinated Infrastructure Network (NNCI) under Award Number ECCS-1542202.

#### **References:**

- Szczech, J. B.; Megaridis, C. M.; Zhang, J.; Gamota, D. R. Ink Jet Processing of Metallic Nanoparticle Suspensions for Electronic Circuitry Fabrication. *Microscale Thermophys. Eng.* 2004, 8 (4), 327–339.
- Perelaer, J.; Smith, P. J.; Mager, D.; Soltman, D.; Volkman, S. K.; Subramanian, V.; Korvink, J.
  G.; Schubert, U. S. Printed Electronics: The Challenges Involved in Printing Devices,
  Interconnects, and Contacts Based on Inorganic Materials. J. Mater. Chem. 2010, 20 (39), 8446.
- (3) Chang, W. Y.; Fang, T. H.; Sheh, Y. T.; Lin, Y. C. Flexible Electronics Sensors for Tactile Multiscanning. *Rev. Sci. Instrum* **2009**, *80*, 084701–084716.
- (4) Rida, A.; Yang, L.; Vyas, R.; Bhattaeharya, S.; Tentzeris, M. M. Design and Integration of Inkjet-Printed Paper-Based UHF Components for RFID and Ubiquitous Sensing Applications. *Proc. 37th Eur. Microw. Conf. EUMC* **2007**, 724–727.
- (5) Angmo, D.; Larsen-Olsen, T. T.; Jørgensen, M.; Søndergaard, R. R.; Krebs, F. C. Roll-to-Roll Inkjet Printing and Photonic Sintering of Electrodes for ITO Free Polymer Solar Cell Modules and Facile Product Integration. *Adv. Energy Mater.* 2013, 3 (2), 172–175.
- (6) Eom, S. H.; Park, H.; Mujawar, S. H.; Yoon, S. C.; Kim, S. S.; Na, S. I.; Kang, S. J.; Khim, D.; Kim, D. Y.; Lee, S. H. High Efficiency Polymer Solar Cells via Sequential Inkjet-Printing of PEDOT:PSS and P3HT:PCBM Inks with Additives. *Org. Electron.* 2010, 11 (9), 1516–1522.
- (7) Mahajan, A.; Frisbie, C. D.; Francis, L. F. Optimization of Aerosol Jet Printing for High Resolution, High Aspect Ratio Silver Lines. ACS Appl. Mater. Interfaces 2013, 5 (11), 4856– 4864.
- (8) Hummelgård, M.; Zhang, R.; Nilsson, H. E.; Olin, H. Electrical Sintering of Silver Nanoparticle Ink Studied by In-Situ TEM Probing. *PLoS One* **2011**, *6* (2), 1–6.
- (9) Francis, L. F. Materials Processing: A Unified Approach to Processing of Metals, Ceramics and Polymers, 1st ed.; Elsevier Inc., 2016.
- (10) Tobjörk, D.; Aarnio, H.; Pulkkinen, P.; Bollström, R.; Määttänen, A. IR-Sintering of Ink-Jet

- Printed Metal-Nanoparticles on Paper. Thin Solid Films 2012, 520 (7), 2949–2955.
- (11) Murphy, C. Radiant Heating With Infrared. 1999, 39.
- (12) Cherrington, M.; Claypole, T. C.; Deganello, D.; Mabbett, I.; Watson, T.; Worsley, D. Ultrafast Near-Infrared Sintering of a Slot-Die Coated Nano-Silver Conducting Ink. *J. Mater. Chem.* 2011, 21 (21), 7562–7564.
- (13) Hwang, H. J.; Chung, W. H.; Kim, H. S. Insitu Monitoring of Flash-Light Sintering of Copper Nanoparticle Ink for Printed Electronics. *Nanotechnology* **2012**, *23* (48).
- (14) UT Dots. Our Products https://utdots.com/products (accessed Aug 8, 2019).
- (15) Zare Bidoky, F.; Frisbie, C. D. Parasitic Capacitance Effect on Dynamic Performance of Aerosol-Jet-Printed Sub 2 V Poly(3-Hexylthiophene) Electrolyte-Gated Transistors. ACS Appl. Mater. Interfaces 2016, 8 (40), 27012–27017.
- (16) Secor, E. B. Guided Ink and Process Design for Aerosol Jet Printing Based on Annular Drying Effects. *Flex. Print. Electron.* **2018**, *3* (3).
- (17) Worldwide, A. adphosNIR technology https://www.adphos.com/technology/adphosnir-technology/ (accessed Jun 8, 2018).
- (18) Mahajan, A.; Francis, L. F.; Frisbie, C. D. Facile Method for Fabricating Flexible Substrates with Embedded, Printed Silver Lines. *ACS Appl. Mater. Interfaces* **2014**, *6* (2), 1306–1312.
- (19) Cai, F.; Chang, Y.; Wang, K.; Khan, W.; Pavlidis, S.; Papapolymerou, J. High Resolution Aerosol Jet Printing OfD- Band Printed Transmission Lines on Flexible LCP Substrate Characterize the DC Performance of the Printed Metal. **2014**, 0–2.
- (20) Vaillancourt, J.; Zhang, H.; Vasinajindakaw, P.; Xia, H.; Lu, X.; Han, X.; Janzen, D. C.; Shih, W.; Jones, C. S.; Stroder, M.; Chen, M. Y.; Subbaraman, H.; Chen, R. T.; Berger, U.; Renn, M. All Ink-Jet-Printed Carbon Nanotube Thin-Film Transistor on a Polyimide Substrate with an Ultrahigh Operating Frequency of over 5 GHz All Ink-Jet-Printed Carbon Nanotube Thin-Film Transistor on a Polyimide Substrate with an Ultrahigh Operating Frequency O. Appl. Phys. Lett. 2008, 93, 243301.

(21) Williams, B. A.; Mahajan, A.; Smeaton, M. A.; Holgate, C. S.; Aydil, E. S.; Francis, L. F. Formation of Copper Zinc Tin Sulfide Thin Films from Colloidal Nanocrystal Dispersions via Aerosol-Jet Printing and Compaction. ACS Appl. Mater. Interfaces 2015, 7 (21), 11526–11535.